Appl. Phys. A 68, 275–282 (1999)

Applied Physics A
Materials
Science & Processing

Spectroscopic properties and STM images of carbon nanotubes

A. Rubio

Departamento de Física Teórica, Universidad de Valladolid, E-47011 Valladolid, Spain

Received: 23 November 1998/Accepted: 22 December 1998

Abstract. We present a theoretical study of the role of the local environment in the electronic properties of carbon nanotubes: isolated single- and multi-wall nanotubes, nanotube ropes, tubes supported on gold and cut to finite length. Interaction with the substrate or with other tubes does not alter the scanning tunneling microscopy patterns (STM) observed for isolated tubes. A finite-length nanotube shows standing-wave patterns that can be completely characterized by a set of four different three-dimensional shapes. These patterns are understood in terms of a simple π-electron tight-binding (TB) model. STM-topographic images of topological defects ani (pentagon/heptagon pair) and tube caps have also been studied. In both cases the image obtained depends on the sign of the applied voltage and can be described in terms of the previous catalog of STM images (interference between electronic waves scattered by the defect). We have also computed the electronic density of states for isolated tubes with different chiralities and radii, confirming a correlation between the peak structure in the DOS and nanotube diameter. However, the metallic plateau in the DOS also depends on the nanotube chirality. Furthermore the conduction an valence band structures are not fully symmetrical to one another. This anisotropy shows up in the DOS and indicates the limitations of the π-TB model in describing spectroscopic data. In contrast to STM images, here the interaction with the substrate does modify the energy levels of the nanotube. We observe opening of small pseudogaps around the Fermi level and broadening of the sharp van Hove singularities of the isolated single-walled nanotubes that can be used to extract useful information about the tube structure and bonding. The combination of STM and spectroscopic studies provides a new way to address the electronic and structural properties of carbon and composite nanotubes.

PACS: 71.20.Tx; 81.05.Tp; 71.15.Fv

Carbon is an extraordinary element that appears in a wide variety of network-like structures with new potential technological applications [1–4]. Among these new forms, carbon nanotubes [5] are the most promising class of new carbon-based materials for electronic and optic nanodevices as well as composite reinforcement materials. The quasi-one-dimensional structure and crystallinity of the sample is responsible for the unique electronic and mechanical properties of carbon nanotubes. The special geometry makes the nanotubes excellent candidates for use as nanoscopic quantum wires.

The type of nanotube obtained experimentally depends on the synthesis conditions and whether a catalytic metal particle is used or not. Multiwall nanotubes (MWNT) have diameters usually in the range 1–25 nm and are many microns in length, whereas single-wall nanotube (SWNT) synthesis requires catalytic particles and SWNTs have diameters in the range of 0.6–2 nm [6, 7]. SWNTs are rarely seen as individual entities and they tend to appear in the form of "ropes", that usually consist of up to a hundred mono-disperse nanotubes packed in a perfect triangular lattice. Experiments (both dual pulsed-laser [6] and standard electric arc techniques [7]) show that the nanotubes forming these ropes often have a diameter of approximately 1.3 nm [6, 8].

Single-wall carbon nanotubes can de described as single graphene sheets wrapped into seamless cylinders. This structure is completely determined by two integer numbers (n, m) that define the circumferential vector $(\mathbf{c} = n\mathbf{a}_1 + m\mathbf{a}_2)$ with respect to the two Bravais translation vectors of a graphene sheet. The electronic properties of carbon nanotubes are dictated by their geometry with either semiconducting or metallic behavior [9]. In particular, the armchair (n, n) nanotube with its n mirror planes containing the tubular axis has an atomic periodicity along the tubular axis of $a = 2.46$ Å and is expected to be metallic with two π bands crossing at the Fermi level. The relation between nanotube chirality and its electrical properties can be complementarely explored by theoretical calculations and scanning tunneling microscopy (STM) experiments, since it allows both topographic imaging and scanning tunneling spectroscopy (STS) from which information about the local density of states (LDOS) can be obtained. Interactions stemming from tube-packing or the tube/substrate/tip can modify the predicted

properties of isolated SWNT and need further study and detailed analysis [10].

The study of electron standing waves (SW) is of fundamental interest as one directly addresses theoretical and experimental problems connected with low-dimensional systems (quasi-one-dimensional molecular wires). Aspects such as Coulomb blockade, localization, oscillations in the conductivity and the quantized conductance (in units of the conductance quantum $G_0 = 2e^2/h = (12.9\,\text{kiloohms})^{-1}$) of nanotubes have already been observed [11–13]. In this last case, the nanotubes conduct current ballistically and do not dissipate heat. The transition from one-dimensional (1D) to zero-dimensional (0D, quantum-dot) systems can be studied by looking at different finite-length carbon nanotubes [8, 14]. If a conducting nanotube is cut to a finite length, the electrons should then display the standing waves characteristic of a 1D particle-in-a-box model. Evidence for 1D quantum confinement was already obtained from transport measurements on single-wall tubes [11, 16], but the standing-wave states have only recently been observed in 1D STS scans [8] and described theoretically [14].

In the present work we present large-scale ab initio and simple tight-binding (TB) calculations of the electronic properties (density of states and STM imaging) of different carbon nanotube structures: chiral and non-chiral SWNT, three-layer MWNT and a three-tube bundle (the simplest nanotube rope), tubes with defects and finite-length tubes. The STM images show no drastic dependence on the different local environment of the tube and can be easily described in terms of a simple TB model. This is important for routine studies of geometrical effects in the experimental images [14, 15]. In the case of finite armchair tubes deposited on a gold surface we present the energies and three-dimensional shapes of 1D standing-wave states, which can be characterized in terms of a simple 'catalog' consisting of only four different patterns. Furthermore, we confirm that all semiconducting tubes with similar diameters have a similar DOS around the Fermi level [17, 18], but there are some particular exceptions. The strucrure in the DOS for the smaller semiconducting and metallic nanotubes shows a dependence not only on the nanotube diameter but also on the nanotube chirality. The interaction between tubes in a bundle tends to open a small pseudogap in the Fermi level [19] and to smooth out the peak structure in the DOS, making the electron–hole asymmetry clearer.

1 Theoretical model

Briefly, we have performed the ab initio calculations using the standard plane-wave pseudopotential total-energy scheme [20, 21] in the local density approximation (LDA) [22] to the exchange correlation potential. Ab initio norm-conserving nonlocal ionic pseudopotentials have been generated by the soft-pseudopotential method of Troullier and Martins [23]. The LDA wave functions were expanded in plane waves up to a 48-Ry cutoff (see [20, 21] for details of the method). In studise of finite-length tubes, the large unit cell together with the large number of atoms involved ($\simeq$ 1000) makes the plane-wave calculation prohibitive. In this case we made calculations in a localized atomic-orbital basis set [24]. The scheme includes order-N algorithms that allow relatively fast calculations with several hundred atoms in the unit cell and has already been applied successfully in studying electronic, structural and STM images of carbon nanotubes [14, 25].

The STM topographic images were simulated within the Tersoff–Hamann theory [26]. In this model the tip is not taken into account explicitly, therefore convolution effects due to the tip shape are neglected. The STM current for an external applied bias voltage V is proportional to the spatially resolved local density of states (LDOS) integrated between the Fermi level of the tip and sample:

$$I(\boldsymbol{r}, V) = \int_{\epsilon_\mathrm{F}-V}^{\epsilon_\mathrm{F}} \mathrm{d}E\ \rho_\mathrm{LDOS}(\boldsymbol{r}, E)\ , \tag{1}$$

with

$$\rho_\mathrm{LDOS}(\boldsymbol{r}, E) = \sum_i |\ \psi_i(\boldsymbol{r})\ |^2\ \delta(E_i - E)\ , \tag{2}$$

where ψ_i, E_i are the electron wave function and eigenvalue of state i, respectively. We then approximate the constant current images as isosurfaces of $I(\boldsymbol{r}, V)$. A description in which the tip is treated as a single s atom has been shown to be important in describing the correct shape and relative intensities in the topographic images [15]. Moreover, the differential conductance $\mathrm{d}I/\mathrm{d}V$, as measured in scanning tunneling spectroscopy experiments, gives direct information about the wave-function square amplitude and, therefore, has direct access to the electronic level structure. In practice, two limiting factors determine the imaging of standing-wave patterns: one extrinsic factor due to the experimental energy resolution (smaller than the molecular level spacing) and another intrinsic factor related to the electron lifetime of the molecular state (SW). Recent calculations show that conduction electrons in armchair nanotubes have very large electron mean free paths, resulting in exceptional ballistic transport and localization lengths of 10 μm [27]. Therefore the main scattering at low experimental temperatures ($T \approx 4$ K) for short tubes stems from the tube boundaries and/or defects and should be small, making the observation of single molecular orbitals possible [8, 14].

For armchair tubes we have performed a complete study of the STS images within the usual tight-binding model for a π-bonded graphene sheet [1]. In this model we retain only nearest-neighbor interaction between p_z orbitals oriented perpendicular to the tube axis. The Hamiltonian is $H_{ij} = -\gamma_0$ for nearest-neighbor atoms, and $H_{ij} = 0$ otherwise and it is known to provide an excellent description of the low-energy features for isolated armchair nanotubes [9, 28], when $\gamma_0 \sim 2.7$ eV. This model can be solved analytically. In Fig. 1 we present the four wave-function patterns obtained by combining the bonding and antibonding solutions with the sine and cosine envelopes for electronic states close to the Fermi level. They constitute the *complete catalog* of the STS patterns to be expected near the Fermi level at the center of the armchair nanotube. This simple prediction of the TB model is confirmed by ab initio calculations [14] to be presented below and give us confidence in using the TB model to describe low-energy properties of other metallic and semiconducting tubes. The predicted catalog of only *four* 3D STM patterns should be confirmed experimentally and extended to other tube chiralities in the future.

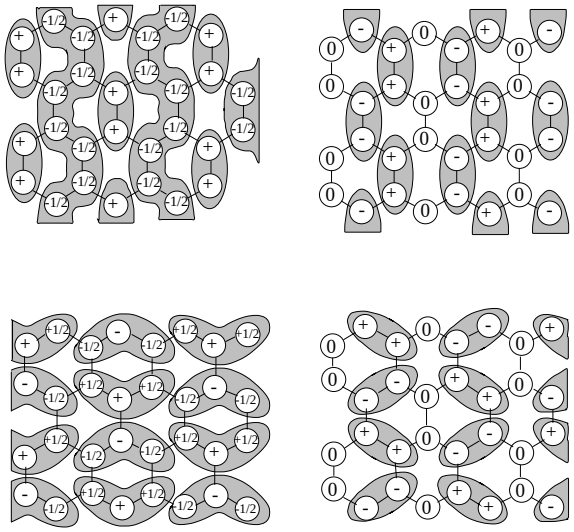

Fig. 1. Schematic tight-binding catalog of STS images for an armchair nanotube close to the Fermi level. It corresponds to the bonding and antibonding $\sin(kz)$ and $\cos(kz)$ solutions in a 1D-confinement-box model (the wave-function values are indicated by the + and − symbols). The general solution for a finite-length, L, tube is given by a combination of sine and cosie functions with the same character. In fact a change in length from L to $L \pm a/2$, a being the lattice parameter along the tube axis, corresponds to a shift in the image pattern. The same scheme holds for supported tubes on a gold (111) substrate

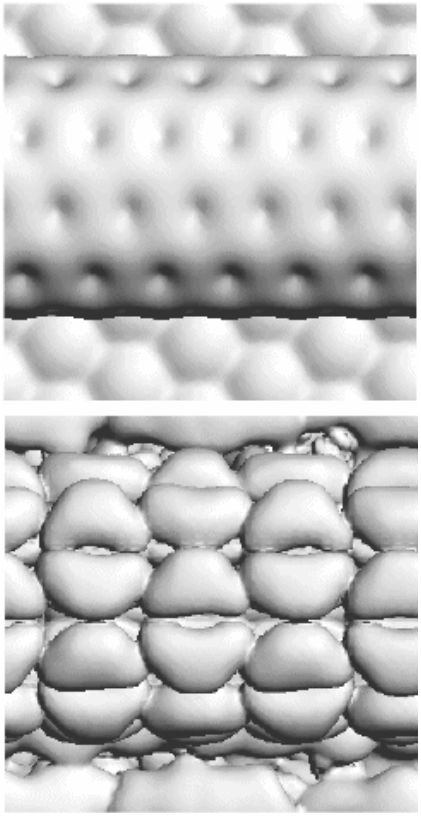

Fig. 2. Ab initio calculation for a (5,5) carbon nanotube supported on Au(111): *Top*, STM topographic image for an applied voltage of 2 eV. *Bottom*, standing-wave pattern of the highest occupied molecular orbital (HOMO). This SW pattern fits one in the catalog of STS images in Fig. 1, showing the marginal role of the substrate in defining the STS images of states close to the Fermi level of the supported tube

2 Theoretical STM images

2.1 Infinite long tubes: SWNT, MWNT and bundles

Scanning tunneling microscopy experiments have resolved the atomic structure and confirmed the predicted interplay between geometry and electronic properties [29]. However, the determination of the diameter of the nanotube is not straightforward due to tip-convolution effects and operation mode [30]. The chiral angle can be affected by mechanical distortions [31] and by the geometry of the STM experiment in obtaining the topographic image: the cylindrical geometry of the nanotube produces a geometrical distortion of the image stretched in the direction perpendicular to the tube axis [15]. Our ab initio calculations for the shape of free-standing isolated SWNTs support the results obtained by a much simpler tight-binding model [15]. The present work gives some information about the influence of tube–tube and tube–substrate interactions in bundles of tubes (nanotube ropes) and in multiwall nanotubes that are beyond the capabilities of semi-empirical models.

Many STM experiments are performed on supported tubes on substrates, therefore it is important to get insight into the role played by the substrate in the experimental images. We performed first-principles calculations for a (5,5) carbon nanotube supported Au(111) surface (see footnote 1) as in the experiments [8]. The gold substrate modifies the spectrum in several ways. (i) It opens a small "pseudogap" in the tube states at the Fermi level whenever the symmetries of the tube are not respected by the gold substrate [19], as in this case where the mirror symmetry of the nanotube is destroyed by the substrate. This symmetry is responsible for the metallic behavior of the armchair nanotubes and breaking it would alter its electronic properties. (ii) It shifts the Fermi level producing a transfer from the gold to the nanotube and quite a strong tube–substrate bonding that prevents the tube from moving (binding energy of about 1.2 eV per tube unit cell). More important for STM imaging is the fact that the charge transfer does not change the SWNT image catalog of Fig. 1. This can be seen in Fig. 2 where we show the computed charge density and STS images for a state close to the Fermi level for the supported nanotube. Furthermore, by looking in detail at all states close to the Fermi level, we observe that the shape and general form of the wave functions matched the previously discussed patterns for unsupported tubes [14]. Although these studies were performed for periodic tubes, we expect the same results to hold for finite-length supported tubes (see below and [14] for more details). The fact that states a few tenths of eV above/below the Fermi level are not resolved experimentally [8] supports our observation that the validity of the two-band model for the electronic structure of an isolated SWNT is destroyed by the strong interaction between the unoccupied ascending band of the tube and the Au(111) surface state.

Now we focus on how tube–tube interactions modify the previous STM patterns. In Fig. 3 we present the results of the calculated 3D-STM image is obtained for an external voltage of $+0.5$ eV for a bundle made of three (8,8) nanotubes and for a three-wall MWNT made of (5,5), (10,10) and (15,15) concentric nanotubes. We have only relaxed the structure of the isolated SWNTs. Then the bundle is formed by packing

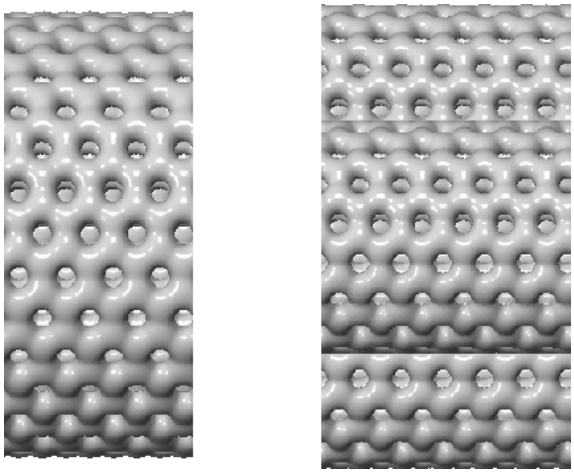

Fig. 3. STM topographic image computed at an external applied bias of $+0.5$ eV. *Left*, for a MWNT formed by three concentric shells of armchair tubes: $(5,5)+(10,10)+(15,15)$ of diameters 0.68, 1.36 and 2.05 nm, respectively. *Right*, corresponds to a tube bundle formed by three (8,8) armchair tubes (of ~ 1.1 nm diameter). In all cases the tube–tube distance is very close to the corresponding graphitic value (0.34 nm)

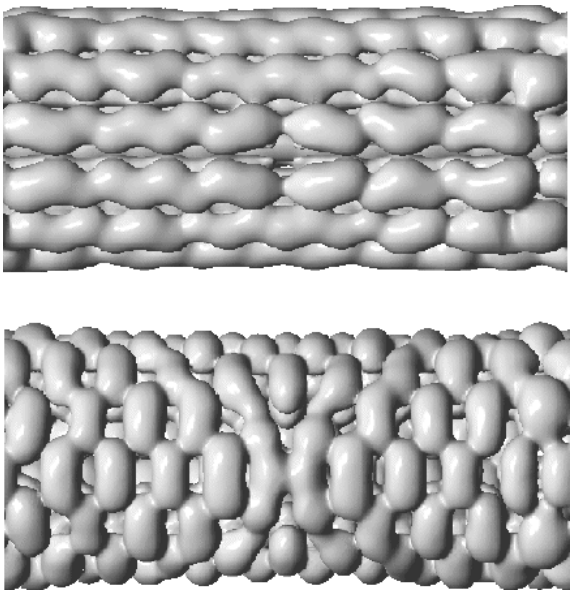

Fig. 4. STM topographic images of a (6,6) carbon nanotube with a pentagon–heptagon pair oriented along the tube circumference with the pentagons aligned with the tube axis. *Top* (*bottom*) figure corresponds to an external applied voltage of -0.5 ($+0.5$) eV. We see a strong dependence on the bias voltage reproducing some of the TB patterns of the complete catalog shown in Fig. 1

the SWNTs, keeping the tube distance close to the graphitic value. We checked that changing the polarity of the applied voltage does not introduce appreciable changes in the STM topographic image. Even for the isolated tubes, the curvature somehow makes visible the asymmetry of the two inequivalent carbon atoms in a graphitic structure. This effect is not of great importance for the topmost atoms and gets more striking as we move along the circumference of the tube. However, the atomic corrugation would be hidden by the much larger geometrical corrugation of the object that the tip must follow. This is relevant in getting the usual 2D-STM topographic maps [15]. We are extending this study to more complex situations including tip-convolution effects [32].

2.2 Topological defects and caps

Defects are expected to be present in nanotubes in several forms: doping and topological defects, hybridisation and incomplete bonding. The presence of such defects could substantially alter both the electronic and elastic properties of nanotubes. Topological defects as the Stone–Wales transformation (pentagon–heptagon pair obtained by a $\pi/2$ rotation of one bond in a four-hexagon complex) are difficult to observe in transmission electron microscope experiments, given that they conserve the curvature of the tube. Depending on the tube symmetry, either metalization or band-gap opening can result. In the case of (n,n) tubes a line of allowed k values runs from γ_0 to K in the graphite-extended zone, moving the Fermi level along this line from K to γ_0 upon introduction of rotated-bond defects should not open a gap. Instead, an increase of approximately 25% in the density of states at the Fermi level should be expected, as the $\pi-\pi^*$ band dispersion decreases [33]. Therefore, STM experiments might give valuable information about these topological effects. Along this line we present in Fig. 4 the computed image of a (6,6) nanotube with a topological Stone–Wales defect for two different applied voltages ± 0.5 eV. The geometry of the defect has been relaxed by assuming periodic boundary conditions with an unit-cell length of 2.5 nm. The total-charge density has an accumulation (deficiency) of charge on the pentagon (heptagon) site that has importance in the use of nanotubes for electro-chemical applications [34].

Some clear effects are observed from the calculations shown in Fig. 4. (i) The STS images fall into one of the patterns predicted by the simple TB model in Fig. 1 and different external applied voltages select specific states of the catalog. (ii) Due to the mirror symmetry along a plane perpendicular to the tube axis of the pentagon–heptagon-pair defect, the wave-function pattern is identical on both sides of the defect. This would not be the case for other relative orientations of the defect. A more complex structure has been predicted in [15] for a single pentagon/heptagon defect joining a metallic and semiconducting tube; the perturbation dies out much faster in the semiconducting side than on the metallic one. We note that localized-defect states as well as tip states have already been observed in STS experiments [35] and our calculations show that the Stone–Wales defect can, indeed, be experimentally accessible by STS measurements and 3D mapping. Physically we can interpret these patterns as the result of an interference effect between the scattered electron waves by the defect. The STM pattern would be different depending on the symmetry of the defect.

To conclude this section, we show in Fig. 5 the computed STM topographic images for a finite-capped (6,6) tube. The capped geometry consist of a perfect half-fullerene (C_{60}) on one end and an open end saturated with hydrogen atoms to avoid the formation of dangling-bond states. Again we see the formation of an electron standing wave formed by constructive interference between the electronic states around the Fermi level and its reflection on the tube boundaries. The pattern obtained can be described as a linear combination of the simplest TB patterns with some chiral pattern that depends on the geometrical orientation of the pentagons

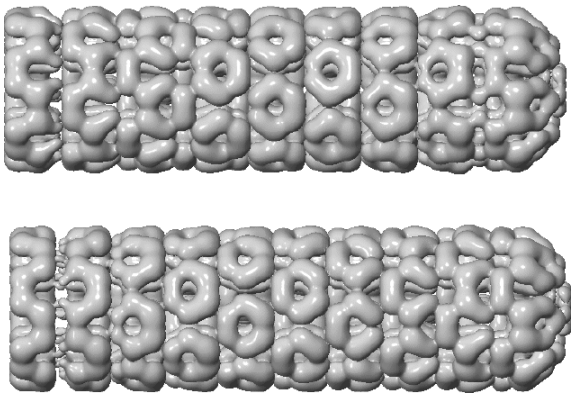

Fig. 5. STM topographic image for a (6,6) capped carbon nanotube of ~ 3.5 nm length. The cap consist of a perfect half-fullerene on one end and an open end saturated with H. *Top* (*bottom*) figure corresponds to an external applied voltage of -0.5 ($+0.5$) eV that in the present case corresponds basically to sampling the LUMO (HOMO) states of the finite system

in the cap. We note again a clear dependence of the topographic image on the external applied voltage due to the different electronic state observed. The scattering at the tube boundaries produces the formation of different standing-wave patterns with a rotational symmetry dictated by the relative position of the pentagons in the cap with respect to the hexagonal network. Standing-wave patterns are also present in the case of finite-length tubes (see below). These complex patterns are similar to the ones expected for chiral carbon nanotubes.

2.3 Finite-size effects: electron standing waves

More detailed information about the electronic structure of 1D quantum wires can be directly obtained in STS experiments by mapping the 1D confinement of electrons in the nanotube structure. This can be achieved by cutting the tube to a finite length [36], which reduces the periodic band structure to a discrete set of molecular levels [37] that can now be imaged by STM [8, 38]. In this simple scenario of a 1D particle-in-a-box model, a tube of length L has a set of allowed ks given by $k = n\pi/L$ (n integer). By taking the Fermi level of the tube at the single graphene-sheet value of $k_{\mathrm{F}} = 2\pi/3a$, the wave functions close to the Fermi level will exhibit a periodic pattern with a wavelength of $\lambda_{\mathrm{F}} = 3a = 0.74$ nm, as observed in STS measurements [8]. Although, this basic standing-wave observation can be explained in terms of the simple 1D particle-in-a-box model, further insight is needed to understand their energy and three-dimensional shape.

The four-image pattern presented in Fig. 1 is fully confirmed by extensive ab initio calculations for SWNT of different lengths and diameters isolated and supported on gold Au(111) [14][1]. In spite of the 'weak' disorder introduced by the interaction with the substrate, our results indicate that the electron images close to the Fermi level fit the same pattern as those of isolated tubes. Furthermore, the experimentally observed effect of peak pairing [8] is explained by the asymmetric shapes of the lobes in the catalog of Fig. 1 [14]. An example of the STM images obtained for a supported (5,5) tube on gold is presented in Fig. 2, where the topographic image for an applied voltage of 1 eV (top) and STS image of the HOMO state (bottom) are given. We confirm the observation of a standing-wave modulation of 0.74 nm near the Fermi level. Also, the peak pairing observed in the experimental scans [8] is understood in view of our calculations [14].

We find that the electronic-state images can be understood in terms of the simple TB model, which offers a catalog of just four image patterns [14]. However, the associated energies are very sensitive to different effects beyond that model: the relaxed geometry, the electronic self-consistency in the finite tubes, and the interaction with the substrate. In general, the value of the HOMO–LUMO gap decreases with increasing tube length not monotonically but exhibiting a well-defined oscillation that is related to the bonding character of the HOMO and LUMO orbitals [37]. By increasing the tube length we observe a smooth transition from an energy-level structure characteristic of a molecular wire (zero-dimensional system) to that of a delocalized one-dimensional system, which seems to be complete for tube lengths of the order or larger than 5 nm [37]. We conclude that tube curvature, termination, structural relaxation, and substrate interaction *do not* significantly alter the simple TB-STM patterns, which therefore should indeed be observed experimentally [14]. However, this is not the case for the level structure that is very relevant for the transport properties of the recently proposed electronic devices based on supported nanotubes.

A general remark should now be made. Troughout this work we have presented 3D-STM images corresponding to a constant-current operational mode in the STM. This data can be accessible experimentally; however, the usual published data correspond to 2D topographic maps of the nanotubes. When bringing our data to the 2D maps care has to be taken due to a geometrical distortion induced by the tip–tube geometry [15]. This geometrically induce distortions prompt us to present our computed STM images in a 3D format.

3 Density of states: STS spectroscopy

A better knowledge of the electronic properties of carbon nanotubes can be obtained by complementing the pevious STM images with spectroscopic data, i.e, density-of-states (DOS) calculations. The DOS can give direct information about the metallic/semiconducting behavior of the tubes and particular insight into the tube–tube or tube–substrate interactions. Information about structural properties and the local environment for a carbon or composite nanotube can be extracted from the computed LDOS [10]. In recent work, the connection between tube-diameter and low-energy features in the DOS has been pointed out [17]. The fact that the electronic DOS for each metallic or semiconducting tube is practically independent of the nanotube chirality is in qualitative agreement with STS experiments [29]. The simple π-electron TB model was used to get this general correlation between the tube diameter and features in the DOS [17]. As we show be-

[1] The Au(111) substrate is described by a six-layer slab. During relaxation the near-neighbor atomic distance of the gold bottom layer was fixed to the bulk value (i.e. 2.88 Å). The computed work function of the surface is 5.01 eV close to the experimental work function ~ 5.3 eV. On top of the relaxed surface we deposited a relaxed (5,5) nanotube with its axis pointing along the (110) surface direction. Although there is no experimental evidence of a special orientation of the supported tubes, we chose this direction for practical purposes in order to get a commensurate tube–substrate unit cell. The tube–substrate distance that minimizes the total energy is ~ 2.5 Å

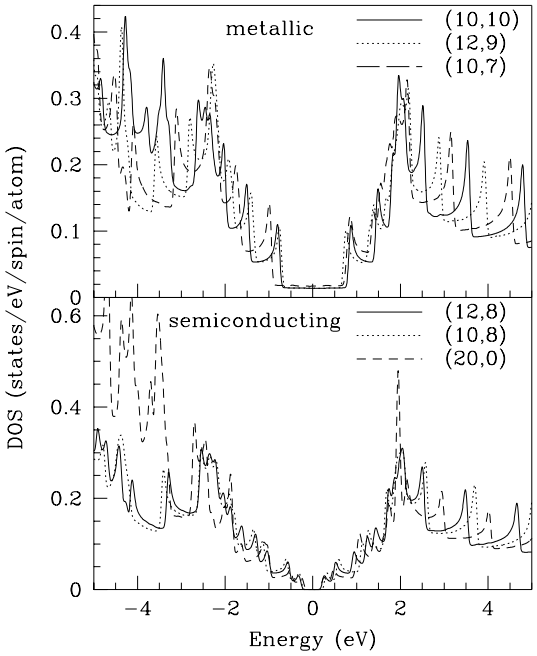

Fig. 6. Ab initio DOS for different metallic and semiconducting tubes with diameters in the range of 1–2 nm, namely: 1.17, 1.36, 1.44, 1.23, 1.37 and 1.58 nm for the (10,7), (10,10), (12,9), (10,8), (12,8) and (20,0) nanotubes, respectively. Spikes in the DOS stem form the van Hove singularities of the nanotube 1D band structure and they play an important role in the description of resonant Raman scattering experiments. All DOS are normalized to the number of atoms in the nanotube unit cell

low, neglect of curvature effects and σ-π hybridization leads to quantitative changes in the DOS in both peak energies and intensities. Therefore, the TB results are valid only for states a few tenths of an eV above or below the Fermi level, and ab initio calculations are needed to address the validity of this simple model.

In an experimental characterization of a carbon nanotube, the DOS plays a key role as can be mapped over a wide range of applied bias. For this reason we plot in Fig. 6 the computed ab initio DOS for a set of chiral and non-chiral tubes with diameters around the experimental value of 1.3 nm (between 1.1 and 1.6 nm). The following conclusions can be extracted from the figure. (i) In metallic tubes the plateau around the Fermi level depends on both tube diameter and, to a lesser extent, on tube chirality. For almost all tubules with a diameter of about 1.3 nm the metallic plateau is about 1.7–2.0 eV. This data is of importance in discriminating metallic and semiconducting tubes in resonant Raman scattering experiments [39, 40]. The non-armchair tubes belonging to the metallic group are indeed quasimetallic with a extremely small gap introduced at the Fermi level by curvature efects. (ii) The electron–hole symmetry of the TB model is no longer valid even for the first spikes in the DOS (see the clear example of the (10,7) metallic tube). This is clearer as the nanotube radius is reduced or/and as we move away from the Fermi level. The separation between van Hove singularities is also slightly different for both conduction and valence states. (iii) The direct connection between the diameter and the structure of the spikes in the DOS is not always clear. Note, for example, that the semiconducting (12,8) and (20,0) nanotubes have very similar DOS close to the Fermi level. However, their diameters are 1.37 and 1.58 nm, respectively. The same holds for the metallic (12,9) and (10,10) tubes with very similar "metallic plateau", but diameters of 1.44 and 1.36 nm, respectively. Then, although the proposal in [17] is very appealing, its practical application to discern the tube diameter is doubtful in its spatial resolution (not better than 0.15 nm for the diameter). In conclusion, to elucidate the geometrical structure of a carbon nanotube we would have to combine spectroscopic and imaging techniques in STM experiments together with simulations.

To get insight into tube–tube interactions in MWNT we plot in Fig. 7 the DOS for a MWNT formed by three concentric armchair tubes such that the inter-tube distance is close to the graphitic value. We see that the low-energy structure seems to give information about the number of layers in the tube. However, this identification gets more complicated when non-commensurate metallic or semiconducting tubes participate as main building blocks of the MWNT. We obtain the expected result that the metallic plateau of the MWNT is mainly controlled by the outer tube (as for the STM images in Fig. 3). The interaction among tubes, being weak, shifts the position of the van Hove singularities in the MWNT with the respect to the SWNT only slightly. This shift is larger for the conduction states, making the electron–hole asymmetry more clear. Modifications due to a finite number of graphene layers with different stacking appear in the DOS as peak structure in the 1–4 eV range. This study was done on a set of graphene layers with different stacking sequences and interlayer distances. Above 3 eV we see the appearance of interlayer and surface states. The results will be reported elsewhere [10, 41].

In Fig. 8 we show calculations for a bundle or nanotube rope conprising three (8,8) SWNT packed on an equilateral triangle network with 0.345 nm intertube distance, aimed at better understanding the role of tube–tube interactions in the DOS. In this case the intertube interaction clearly modifies the spectra seen in the DOS. (i) It opens

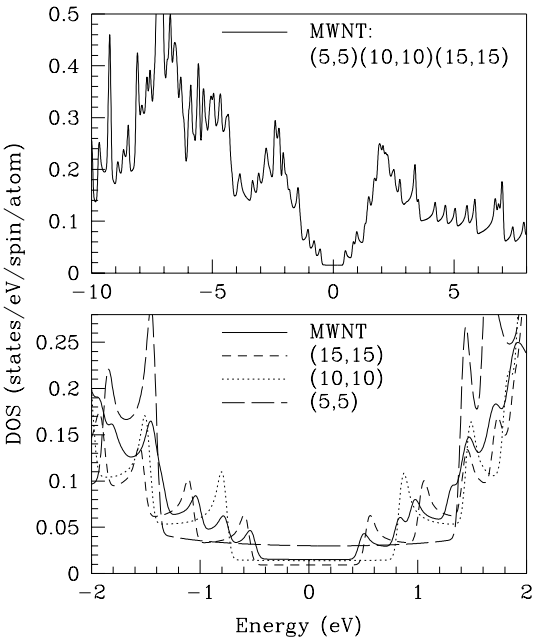

Fig. 7. DOS for a MWNT formed by three concentric armchair tubes: $(5, 5) + (10, 10) + (15, 15)$. *Bottom*, comparison of the DOS for the MWNT with each of the component nanotube DOS magnified around the Fermi level. Each DOS is normalized to the number of atoms in the unit cell

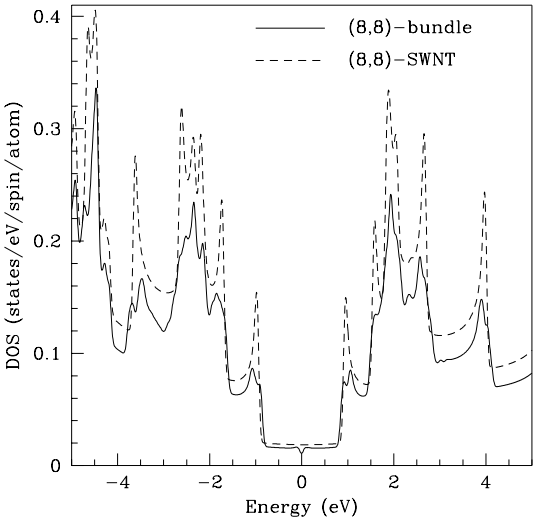

Fig. 8. DOS for a small nanotube rope (bundle) formed by three (8,8) SWNT (1.09 nm diameter) packed in a triangular lattice with an intertube distance of 0.345 nm. We clearly see the opening of a "pseudogap" of about 1 eV around the Fermi level. We compare the results for the bundle with the DOS for an isolated (8,8) SWNT (*dashed line*)

a "pseudogap" close to the Fermi level as already predicted for random-oriented nanotube ropes [19] (pseudogap of ~ 0.1 eV). The bundle remains metallic. (ii) It makes the electron–hole asymmetry in the DOS is more accentuated and the spike structure of the van Hove singularities are smoothed out. The fact that the energy position of the peaks is not strongly modify explains the success of using isolated SWNT spectra to describe the experimental data [29]. However, the shape of the spectra (relative intensities) is strongly affected by tube–tube interactions as is clearly seen in Fig. 8.

To end this section it is worth discussing these results in terms of the simple π electron TB model. Within this simple model the DOS in the vicinity of the Fermi level is symmetric (electron–hole symmetry) and can be expressed in terms of a universal function that depends only on whether the tube is metallic or semiconducting [17]. In terms of the nearest-neighbor overlap energy γ_0 we have that, for a semiconducting tube, the band gap is given by

$$E_{\mathrm{g}} = \frac{2\gamma_0 a_{\mathrm{C-C}}}{D}\,, \tag{3}$$

where $a_{\mathrm{C-C}}$ is the carbon–carbon bond length (~ 1.42 Å) and D is the nanotube diameter. In the case of metallic tubes, the metallic plateau (E_{met}), given by the distance between the two van Hove singularities above and below the Fermi level, is

$$E_{\mathrm{met}} = \frac{6\gamma_0 a_{\mathrm{C-C}}}{D}\,. \tag{4}$$

In both cases the distance between consecutive conduction or valence van Hove singularities is given by $\Delta E = 3\gamma_0 a_{\mathrm{C-C}}/D$. This γ_0 parameter plays an important role in the experimental analysis of their electronic structure data. In fact, a fit to STS experiments [29] gives a value of $\gamma_0 = 2.7$ eV, whereas the fit to resonant Raman scattering experiments on metallic carbon nanotubes [40]gives $\gamma_0 = 2.95 \pm 0.05$ eV. This indirect estimation is in quite good agreement with the direct measurement by STS, and both are smaller than the $\gamma_0 = 3.16$ eV value for graphite [2]. These results stem from the fact that in the TB model we have a radial dependence of the band structure with respect to the Fermi level (K point in the Brillouin zone of the graphene sheet). Our results summarized in Figs. 6, 7 and 8 show that the value of γ_0 is not unique due to the anisotropy of the DOS in both peak positions and intensities. The small band gap of semiconducting tubes makes them the best candidates for experimentally determining the value of γ_0 from (3). The computed values go from 2.77 to 2.95 eV for tubes with diameters of 1.23 and 1.58 nm, respectively. Smaller values are obtained for metallic tubes when fitting the metallic plateau to (4) (from 2.32 to 2.75 eV for diameters of 0.68 to 2.04 nm, respectively). In general, the value of γ_0 increases with increasing nanotube diameter. Furthermore, the interaction between tubes also modify this parameter by as much as 10%[2]. In fact, the electron–hole asymmetry in the DOS is a measure of the curvature effects, intertube interactions and anisotropy in the band structure. Note that because the conduction wave functions are spatially more extended than the valence ones, the unoccupied part of the DOS is more sensitive to any external perturbation (this is clearly seen in Figs. 6, 7 and 8).

4 Summary

We have presented a study of the STM images and electronic properties of carbon nanotubes in different environments. The present technique opens a new way to address the analysis of the interplay between electronic and geometric properties in carbon nanotubes. The method has been applied to SWNT, MWNT and nanotube ropes as well as finite-length armchair nanotubes. Within a very simple TB model we have characterized the complete catalog of STM images as consisting of four images. These results are further confirmed by ab initio calculations. The gold substrate does not alter the main images of the isolated tubes even if the tubes are quite strongly bound to the substrate by charge transfer. The computed images are in very good agreement with experiments in both the wavelength of the standing wave (0.75 nm) and in the inner details (pairing). Surface states related to the boundary of the tubes are observed to appear within 1 eV above the Fermi level. These states could play a role in the field-emission process and chemical activity and for the description of the electronic structure of other chiral tubes (semiconducting) where they can be very close to the bottom of the conduction band. Moreover, different STS patterns are expected for chiral tubes that can be used as a further check of the particle-in-a-box model. Spectroscopic studies based on looking at the DOS gives additional information about the metal/semiconductor character, packing and tube–tube interactions. In this respect, most of the peak structures for the composite DOS can be understood in terms of the isolated SWNTs DOS. However,

[2] The determination of γ_0 turns out to depend on the experimental conditions and model used to extract its value (it is no longer unique but rather model dependent). Note that the DOS for the nanotube bundle in Fig. 8 shows a complex spike structure above and below the Fermi level. Depending on which peak pair is used to fit (4) we get variations of 10% above and below the γ_0 value for the isolated (8,8) SWNT ($\gamma_0 \simeq 2.5$ eV).

subtle but important differences appear in the intensity and shape of the peaks as well as in the opening of a pseudo-gap close to the Fermi level and modification of the effective metallic plateau. These studies nicely complement the STM imaging and provide us with a lot of information that can be checked by experiments.

Acknowledgements. We acknowledge financial support from DGES (Grants: PB95-0720 and PB95-0202) European Community TMR contract ERBFMRX-CT96-0067 (DG12-MIHT). Computer time was provided by the C^4 (Centre de Computació i Comunicacions de Catalunya). We thank C. Dekker, L.C. Venema and D.L. Carrol for sharing their experiments with us prior to publication and for enlightening discussions. We also benefited from fruitful collaborations with E. Artacho, E. Hernández, Ph. Lambin, M.J. López, V. Meunier, P. Ordejón, D. Sánchez-Portal and J.M. Soler.

References

1. Special issues on *Nanotubes* in Carbon **33** (1996); J. Appl. Phys. A **67** (1998)
2. M.S. Dresselhaus, G. Dresselhaus, P.C. Eklund: *Science of Fullerenes and Carbon Nanotubes* (Academic Press, San Diego 1996)
3. T.W. Ebbesen: *Carbon Nanotubes: Preparation and Properties* (CRC, New York 1997)
4. A. Rubio: Cond. Matt. News **6**, 6 (1997); and references therein
5. S. Iijima: Nature **354**, 56 (1991)
6. A. Thess, R. Lee, P. Nikolaev, H. Dai, P. Petit, J. Robert, C. Xu, Y.H. Lee, S.G. Kim, A.G. Rinzler, D.T. Colbert, G.E. Scuseria, D. Tomanek, J.E. Fisher, R.E. Smalley: Science **273**, 483 (1996)
7. C. Journet, W. Maser, P. Bernier, A. Loiseau, P. Deniard, S. Lefrant, R. Lee, J. Fischer: Nature **388**, 756 (1997)
8. L.C. Venema, J.W.G. Wildöer, S.J. Tans, J.W. Janssen, L.J. Hinne, T. Tuinstra, L.P. Kouwenhoven, C. Dekker: Science, **283**, 52 (1999)
9. N. Hamada, S. Sawada, A. Oshiyama: Phys. Rev. Lett. **68**, 1579 (1992)
10. E. Hernández, A. Rubio: (work in progress)
11. S.J. Tans, M.H. Devoret, H. Dai, A. Thess, R.E. Smalley, L.J. Geerligs, C. Dekker: Nature **386**, 474 (1997)
12. S. Frank, P. Poncharal, Z.L. Wand, W.A. de Heer: Science **280**, 1774 (1998)
13. P.G. Collins, A. Zettl, H. Bando, A. Thess, R.E. Smalley: Science, **278**, 100 (1997); S.J. Tans, A.R.M. Verschueren, C. Dekker: Nature **393**, 49 (1998)
14. A. Rubio, D. Sanchez-Portal, E. Artacho, P. Ordejón, J.M. Soler: submitted for publication
15. V. Meunier, Ph. Lambin: Phys. Rev. Lett., **81**, 5588 (1998)
16. M. Bockrath, D.H. Cobden, P.L. McEuen, N.G. Chopra, A. Zettl, A. Thess, R.E. Smalley: Science **275**, 1922 (1997)
17. C.T. White, J.W. Mintmire: Nature **394**, 29 (1998)
18. J.C. Charlier, Ph. Lambin: Phys. Rev. B **57**, R15037 (1998)
19. P. Delaney, H.J. Choi, J. Ihm, S.G. Louie, M.L. Cohen: Nature **391**, 466 (1998)
20. M.L. Cohen: Solid Stat. Commun. **92**, 45 (1994); Phys. Scri. **1**, 5 (1982); J. Ihm, A. Zunger, M.L. Cohen: J. Phys. C **12**, 4409 (1979)
21. W.E. Pickett: Comput. Phys. Rep. **9**, 115 (1989); M.C. Payne, M.P. Teter, D.C. Allan, T.A. Arias, J.D. Joannopoulos: Rev. Mod. Phys. **64**, 1045 (1992)
22. D.M. Ceperley, B.J. Alder: Phys. Rev. Lett. **45**, 1196 (1980); J.P. Perdew, A. Zunger: Phys. Rev. B **23**, 5048 (1981)
23. N. Troullier, J.L. Martins: Solid State Commun. **74**, 613 (1990); Phys. Rev. B **43**, 1993 (1991)
24. D. Sánchez-Portal, P. Ordejón, E. Artacho, J.M. Soler: Int. J. Quantum Chem. **65**, 453 (1997); P. Ordejón, E. Artacho, J.M. Soler: Phys. Rev. B **53**, R10441 (1996)
25. D. Sánchez-Portal, E. Artacho, J.M. Soler, A. Rubio, P. Ordejón: submitted for publication
26. J. Tersoff, D. Hamann: Phys. Rev. Lett. **50**, 1998 (1983)
27. C.T. White, T.N. Todorov: Nature **393**, 240 (1998)
28. J.W. Mintmire, B.I. Dunlap, C.T. White: Phys. Rev. Lett. **68**, 631 (1992)
29. J.W.G. Wildöer, L. C. Venema, A.G. Rinzler, R.E. Smalley, C. Dekker: Nature **391**, 59 (1998); T.W. Odom, J.-L. Huang, P. Kim, C.M. Lieber: Nature **391**, 62 (1998)
30. J. Muster, M. Burghard, S. Roth, E. Hernández, A. Rubio: J. Vac. Sci. Technol. **16**, 2796 (1998)
31. W. Clauss, D.J. Bergeron, A.T. Johnson: Phys. Rev. B **58**, R4266 (1998)
32. V. Meunier, Ph. Lambin, E. Hernández, A. Rubio: (work in progress)
33. V.H. Crespi, M.L. Cohen, A. Rubio: Phys. Rev. Lett. **79**, 2093 (1997)
34. P.J. Britto, K.S.V. Santhanam, A. Rubio, J.A. Alonso, P.M. Ajayan: Adv. Matt. (in press)
35. D.L. Carroll, P. Redlich, P.M. Ajayan, J.C. Charlier, X. Blase, A. De Vita, R. Car: Phys. Rev. Lett. **78**, 2811 (1997)
36. L.C. Venema, J.W.C. Wildöer, T. Tuinstra, C. Dekker, A.G. Rinzler, R.E. Smalley: Appl. Phys. Lett. **71**, 2629 (1997)
37. H.-Y. Zhu, D.J. Klein, T.G. Schmalz, A. Rubio, N.H. March: J. Phys. Chem. Solids **59**, 417 (1997). The band-gap behavior can be divided into four classes depending of the tube length, chirality and capping geometry: (i) The gap diminished toward the infinite-tubule value with a period-3 oscillation of amplitude quenched as $1/L$; (ii) The gap diminished monotonically as $1/L$ to the infinite value; (iii) The gap approaches exponentially fast a constant value different than that for the infinite tubule and (iv) The gap is constant
38. M.F. Crommie, C.P. Lutz, D.M. Eigler: Science **262**, 218 (1993)
39. A.M. Rao, E. Ritcher, S. Bandow, B. Chase, P.C. Eklund, K.A. Williams, S. Fang, K.R. Subbaswamy, M. Menon, A. Thess, R. Smalley, G. Dresselhaus, M.S. Dresselhaus: Science **275**, 187 (1997)
40. M.A. Pimenta, A. Marucci, S.D.M. Brown, M.J. Matthews, A.M. Rao, P.C. Eklund, R.E. Smalley, G. Dresselhaus, M.S. Dresselhaus: J. Mater. Res. **13**, 2396 (1998); Phys. Rev. B **58**, R16016 (1998)
41. A. Rubio, D.L. Carroll: (unpublished work)